

---

# Spatially resolved spectroscopic studies of planetary nebulae and their halos

C. Sandin, D. Schönberner, M. M. Roth, M. Steffen, P. Böhm,  
A. Monreal-Ibero

Astrophysikalisches Institut Potsdam, An der Sternwarte 16, D-14482 Potsdam,  
Germany, [CSandin@aip.de](mailto:CSandin@aip.de)

**Summary.** One application where (3D) integral field spectroscopy is useful is when doing detailed measurements of physical structures in the outer parts of extended planetary nebulae (PNe). The outermost light emitting regions, i.e. halos, are less affected by reshaping processes in the nebula than central parts are and can therefore be used to study the final stage of mass loss on the asymptotic giant branch (AGB). Here preliminary results of a larger and more detailed study are being reported for one of the studied objects, viz. NGC 7662. To this goal an automated method has been developed that includes binning of simultaneously observed spectra, a careful subtraction of telluric lines and now also a correction for differential atmospheric refraction. The results show a steep and narrow positive temperature gradient, revealing a hot halo, in confirmation of previous findings. In the view of radiation hydrodynamic models a hot halo can be the product of the passage of an ionization front – equilibrium models do not show such temperature enhancements.

**Key words:** planetary nebulae: individual (NGC 7662) – Instrumentation: spectrographs – Techniques: spectroscopic – Line: profiles

## 1 Introduction

Halos around planetary nebulae are fossil records of the last mass-loss episode at the tip of the AGB. Although important information about the final AGB evolution can be gained already from halo sizes and radial surface brightness distributions, deeper insight can only be gained by a detailed plasma diagnostic which is with conventional techniques only possible for the brighter nebular shells. The purpose of this study is to derive physical properties of halos surrounding PNe in the galactic disk. Halos are of particular interest since they, unlike the brighter inner parts of the PN, have been less affected by reshaping processes like photo-ionization and shocks. Furthermore, the halo is a very weakly emitting region where line intensities can be a thousand times weaker, and less, compared to the central parts. Few lines are consequently visible. Observing these objects is a challenge which exploits the limits of both instrumental and telescope requirements, as well as observing conditions.

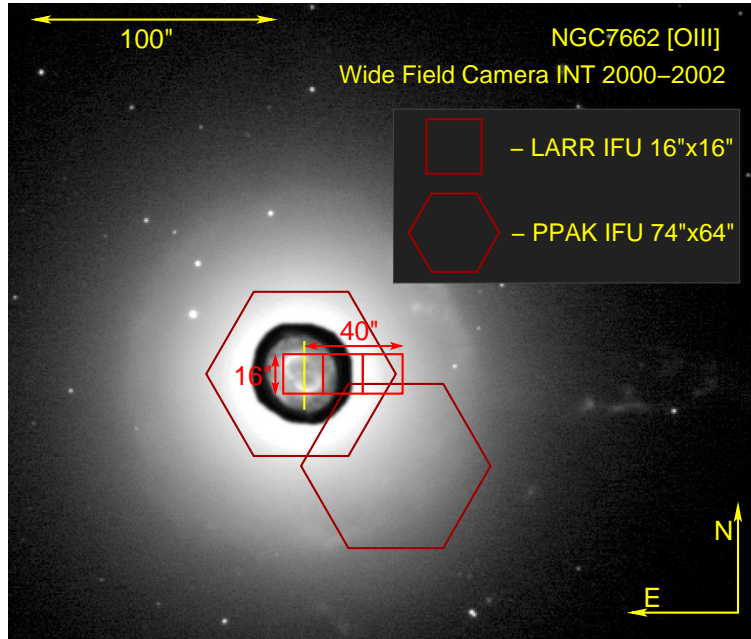


**Fig. 1.** Image of NGC 7662 (from the PN atlas of [3]) showing the extent of a weak – and to a good approximation spherical – halo reaching a radius of about  $70''$ . Grayshades are cyclic to enhance the dynamic range spanning a factor of about  $10^4$ . The location of three PMAS LARR IFU exposures west of the central star is indicated with red boxes. Hexagon outlines indicate how the full radial extent of the halo could be observed in two pointings using the larger PPAK IFU. Also see Fig. 2.

A detailed description of observations, data analysis and results for several nebulae is being prepared in [8]. Here some highlights of that article are presented for NGC 7662. In the following observations and analysis are presented in Sect. 2 and results thereafter in Sect. 3. Section 4 shows how models can be used to explain the results. Finally, conclusions are given in Sect. 5.

## 2 Observations and Analysis

The data of NGC 7662 presented here was obtained in September 2005 using the PMAS spectrograph attached to the 3.5m telescope at Calar Alto. The integral field unit (IFU) used is the lens array (LARR; in the  $1''$  magnification setting) which holds  $16 \times 16$  spatial elements (also called spaxels), each covering a surface of  $1'' \times 1''$ . The wavelength coverage was  $3436\text{--}5093 \text{ \AA}$ , with a spectral resolution of  $3.6 \text{ \AA}$ . Figure 1 shows how three LARR IFU tiles were oriented, covering a strip of the halo  $16'' \times 48''$  large and reaching a distance of  $40''$  from the location of the central star. Data reduction was carried out using the PMAS P3d package [2, 6]. To increase the signal-to-noise spectra of individual spatial elements are binned along

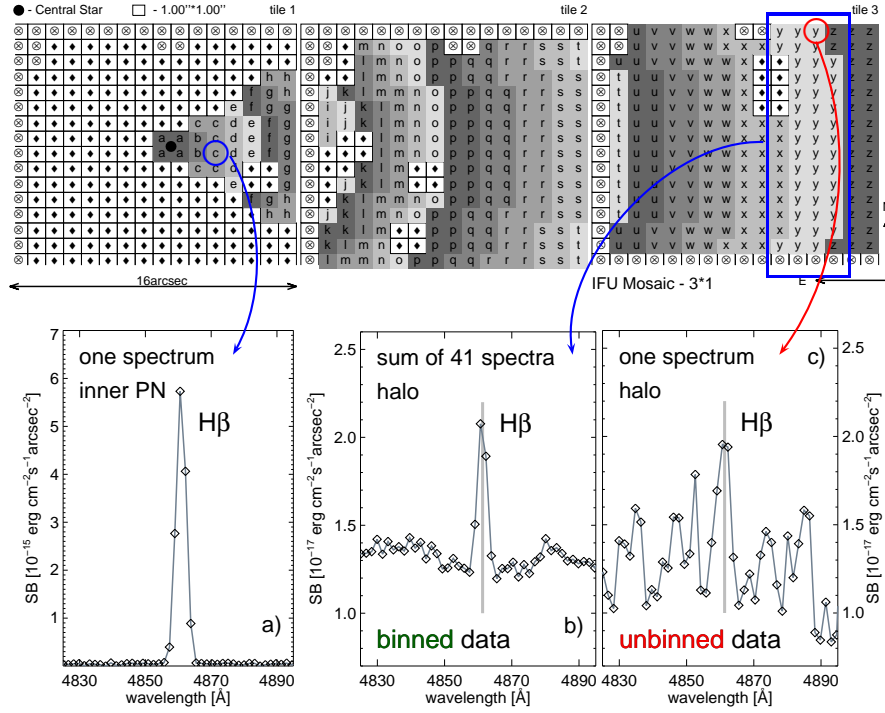


**Fig. 2.** Binning map (top panel) and resulting spectra (bottom panels) from the analysis of NGC 7662. In the top panel each small square represents one spatial element, of  $1'' \times 1''$  size. Totally three tiles with 256 spatial elements each were observed, offset by  $16''$  from each other in the E-W direction (Fig. 1). Spatial elements in concentric arcs (marked with the same letter) are binned, forming one spectrum for each arc and radial location. Spatial elements marked with  $\blacklozenge$  and  $\otimes$  are not used. Remaining panels in the bottom row show the: **a)** raw spectrum of one spatial element in the inner PN; **b)** summed raw spectrum of 41 spatial elements in the halo; and **c)** one raw spectrum of one spatial element in the halo. Errors are for clarity not shown. Arrows indicate where on the IFUs the shown spectra are sampled. Note that the intensity scale of **a)** is different from that in **b)** & **c)**. The latter two panels illustrate how the signal-to-noise of, in this case,  $H\beta$  is increased by binning spectra.

concentric arcs sampling regions of presumably similar properties. How this is done for NGC 7662, which to a good approximation has a spherical halo, is shown in Fig. 2.

For the determination of the electron temperature,  $T_e$ , the three oxygen lines [O III]  $\lambda$  4363,  $\lambda\lambda$  4959, 5007 are used. Due to the close vicinity of [O III]  $\lambda$  4363 to the telluric line Hg  $\lambda$  4358 the latter has to be removed before measuring the object flux. Lacking a separate sky frame a line fit of the sky in this region is first created using a few spatial elements sampling the sky, this sky-fit is then subtracted from all object spectra in this wavelength region.

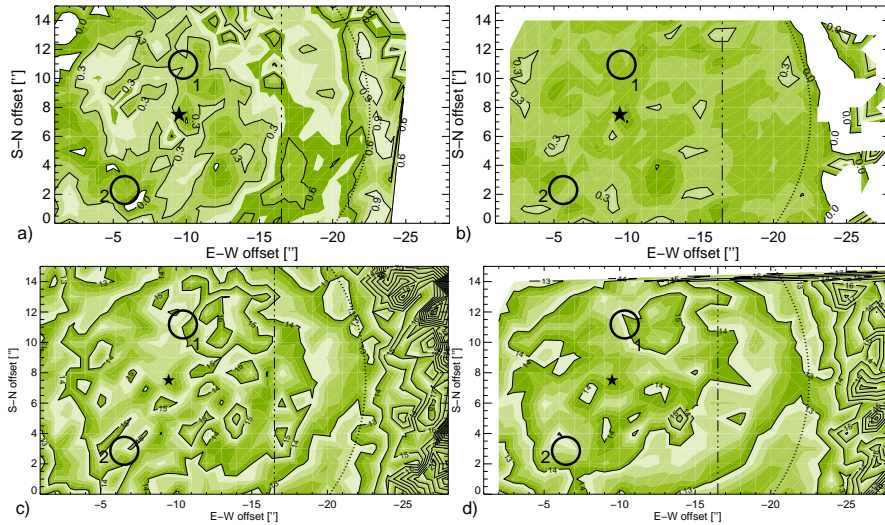


**Fig. 3.** Map of the extinction coefficient  $c$  (upper panels) and electron temperature  $T_e$  (lower panels) for the inner parts of NGC 7662. The left panels a) & c) show derived maps that have not been corrected for DAR, while the right panels b) & d) have been corrected. The location of the central star is marked with the symbol  $\star$  and circles indicate regions also observed by [1] (see table 1). Both upper panels use the same color table. In panels c) & d)  $T_e$  is given in  $10^3$  K. Rows and columns of spatial elements on the N-E most sides in panels b) & d) have been removed during the DAR correction procedure since they depend on flux from unobserved regions outside the IFU. For further details see Sect. 3.

### 3 Results and Discussion

A useful feature of 3D-spectroscopy is that it is straightforward to correct for differential atmospheric refraction (DAR). Due to this refraction photons of different wavelength risk being caught in separate spatial elements. In fact, if observations are carried out at a larger airmass, intensity gradients are present and emission lines of different wavelengths are compared, it is increasingly important to make this correction. In this case the airmass was about 1.3. Illustrating the influence of DAR, maps of the central parts of NGC 7662 for the extinction coefficient  $c$  and electron temperature  $T_e$  are shown in Figs. 3a & c (no DAR correction) and Figs. 3b & d (DAR corrected). When this correction has been applied the rim – seen as a diagonal oval in the center tile in panel a – is less pronounced in  $c$  and the peak where  $c \approx 0.9$  in the inner halo disappears; compare panels a & b at  $E-W \simeq -22''$ . Also the temperature structure changes. The DAR correction procedure decreases the patchiness in both quantities  $c$  and  $T_e$ , an inevitable consequence of the unavoidable spatial interpolation across the IFU.

As Fig. 3 shows neither the extinction coefficient nor the electron temperature map are well determined in the halo; for  $E-W$  offset  $\lesssim -22''$ . To increase the signal-to-noise in these weak regions spatial elements can be binned using maps such as that shown in Fig. 2. Resulting radially binned surface brightness profiles are shown

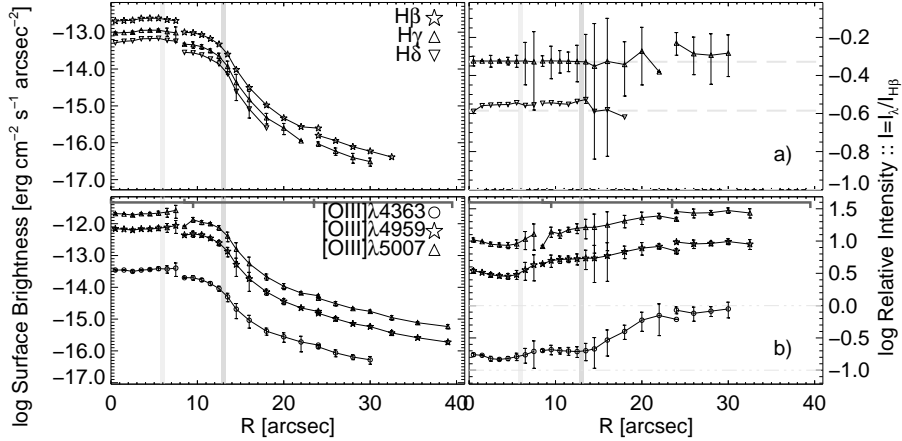


**Fig. 4.** Radial structure of the surface brightness of emission lines of NGC 7662. The panels on the right show the corresponding H $\beta$ -normalized surface brightness. All ordinates are, moreover, logged. The radial locations of the three tiles are indicated in the upper part of the lowermost panel. Top panels (a)) show integrated intensities of Balmer lines, and the bottom panels (b)) oxygen lines. Vertical gray bars indicate the location of the rim, at  $R = 6''$ , and the edge of the shell, at  $R = 13''$ .  $R = 0''$  marks the location of the central star. Error bars show the spaxel-to-spaxel variation (standard deviation) of the intensity of all spatial elements at a certain radius – for clarity not for all lines. In the bottom panel the increase of [O III]  $\lambda$  4363 relative to [O III]  $\lambda\lambda$  4959, 5007 for  $R > 13''$  is due to a temperature increase in the halo. Also note the difference between intensities in the inner PN and halo, reaching a factor of 1000 and larger.

in Fig. 4 for the three oxygen lines, H $\beta$ , H $\gamma$ , and H $\delta$ . Note the large difference in the (log:ed) surface brightnesses between central and outer regions. The intensity-steps between the center and middle tiles seen at  $R \approx 8''$  are due to the asymmetry of the inner nebula; the same steps are smaller at  $R \approx 24''$ . The temperature sensitive line [O III]  $\lambda$  4363 is measurable out to  $R = 30''$ .

The resulting radial electron temperature structure is shown in Fig. 5, both using data not corrected for DAR (right) and corrected data (left; gray lines are also not corrected in this panel). Important to note is the strong temperature gradient in the region  $13'' \leq R \leq 22''$  in which the temperature increases by about 6500 K from the trough in the shell. Also compare to the value measured by [5] (shown with the symbol  $\triangle$  at  $R = 40''$ ). Additionally it is seen that this temperature difference is larger by about  $10^3$  K when the data has been corrected for DAR. There is also a difference compared to [7] where the binning was elementary, no DAR correction was made and the sky subtraction was very simplified.

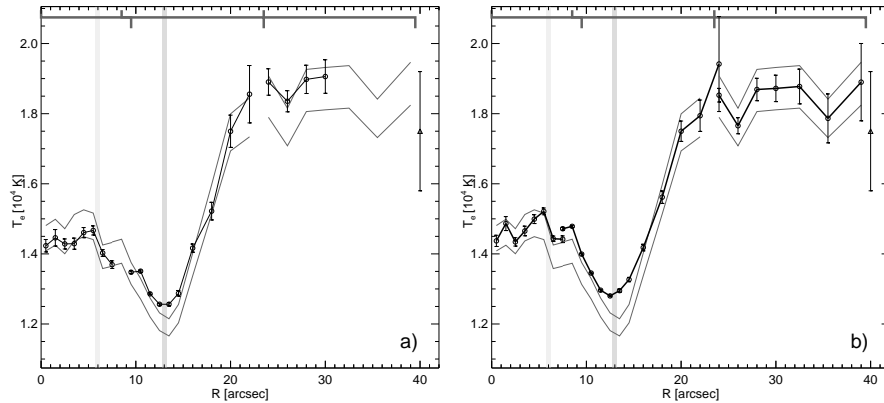


**Fig. 5.** Radial temperature structure of NGC 7662 achieved using the spatial element binning map of Fig. 2. Gray lines (without error bars) were for both panels calculated with a constant extinction coefficient throughout the entire region;  $c = 0.1$  &  $0.4$  for the lower and upper lines, respectively. Black lines were calculated using the variable extinction coefficient of Fig. 3; being constant ( $c = 0.23$ ) for  $R \geq 17''$ . In panel **a**) the black line data was corrected for DAR before calculating the temperature, this was not done for the black line in panel **b**). The difference is the largest for  $10'' \geq R \geq 21''$ . For further details see Sect. 3.

#### 4 Understanding the observations with modeling

An increasing temperature in the halo like that shown in Fig. 5 cannot be explained with a hydrostatic or stationary PN model. However, using a radiation hydrodynamics model it can be explained as a dynamic effect of the passage of an ionization front; that is non-equilibrium heating and cooling immediately after the passage of the ionization front [4, 9]. In Figs. 6a–c such a temporal model sequence is shown for a so-called R-type ionization front covering a period of 125 years (this model has not been chosen to fit the observed properties). The radial region corresponding to the inner halo in Fig. 5 is  $4 \times 10^{17} \lesssim r \lesssim 10 \times 10^{17}$  cm. During the passage of the front the outer halo is being ionized (blue line), simultaneously the temperature changes rapidly by 5000 K in the inner halo. Additionally, note the difference between actual (dashed) and projected (line marked with “\*”) temperatures which is about  $10^3$  K at  $r \simeq 10 \times 10^{17}$  cm.

Clearly, incorrect abundances are obtained in this region when the analysis is based on equilibrium photoionization models which cannot account for the measured temperature enhancement. Moreover, spectroscopic temperatures are affected by projection effects and potentially can also lead to erroneous abundance determinations. Note that since intensities are so low in the outermost halo ( $r > 15 \times 10^{17}$  cm) it will in most cases be very difficult to determine a temperature there. The increase in the density at the edge of the halo at  $r \simeq 15 \times 10^{17}$  cm (solid lines; corresponding to a radius of about  $70''$  in Fig. 1) is seen in an increase of the (modeled) surface brightness of both emission lines in panel **d**).

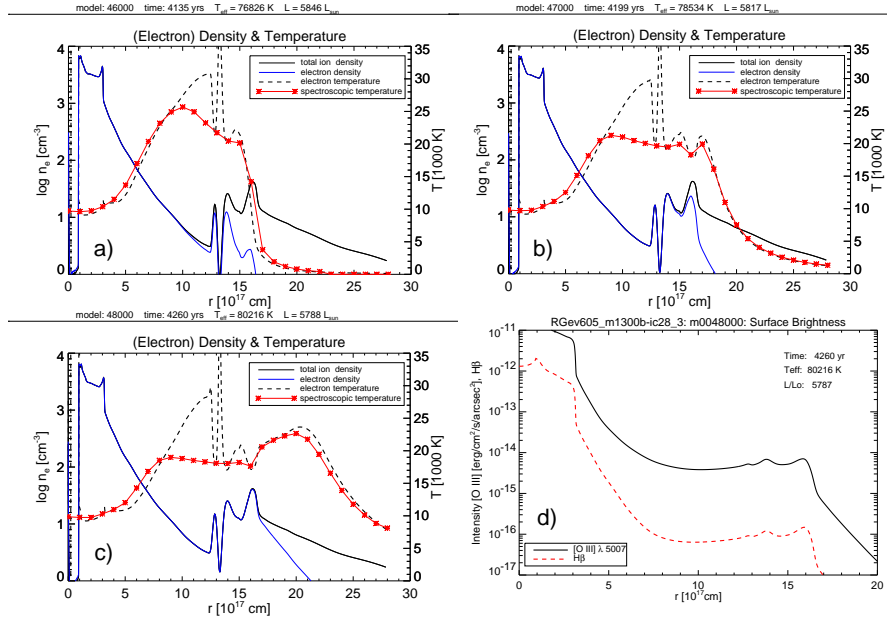


**Fig. 6.** Radiation hydrodynamic model sequence (panels a)–c) showing the evolution of the physical structure in a planetary nebula as the halo is being ionized; the period shown is 125 years long. In panel c) the gradient in the spectroscopic temperature (red line marked with “\*”) for  $4 \times 10^{17} \leq r \leq 10 \times 10^{17}$  cm corresponds to the observed temperature gradient shown in Fig. 5. Panel d) shows two calculated surface brightness curves – like those in Fig. 4 – for instant, c).

## 5 Conclusions

Through the use of 3D spectroscopy observations of physical structures in faint halos of planetary nebulae have become feasible. Such halos are worthwhile observing since they are relatively undisturbed records of the final stages of mass loss on the AGB.

A crucial emission line when determining the electron temperature is [O III]  $\lambda 4363$ , which also is a very weak line. Consequently, an important contribution of 3D spectroscopy is that it allows a binning of spatial elements to increase the observed signal-to-noise in such lines. An improved analysis of the temperature structure in NGC 7662 confirms the presence of a strong temperature gradient in the inner halo. The hot structure, which occurs during the process of photo-ionizing the halo, cannot be explained without a time-dependent model description. Estimates of abundances in the halo, finally, also have the potential of being based on incorrect temperatures if no difference is made between actual and projected temperatures.

*Acknowledgement.* C. S. is supported by DFG under grant number SCHO 394/26. This work is part of the XPN project (<http://www.aip.de/groups/xpn/>)

## References

1. T. Barker 1986, *ApJ* **308**, 314
2. T. Becker 2002, PhD thesis, Univ. Potsdam
3. R. L. M. Corradi, D. Schönberner, M. Steffen, et al. 2003, *MNRAS* **340**, 417
4. H. Marten 1993, *A&A* **277**, 9
5. D. Middlemass, R. E. S. Clegg, J. R. Walsh, et al. 1991, *MNRAS* **251**, 284
6. M. M. Roth, A. Kelz, T. Fechner, et al. 2005, *PASP* **117**, 620
7. C. Sandin, D. Schönberner, M. M. Roth, et al. 2006, in: M. J. Barlow & R. H. Méndez (eds.), *Planetary Nebulae in our Galaxy and Beyond*, Proc. IAU Symposium No. 234, 501
8. C. Sandin, D. Schönberner, M. M. Roth, et al. 2008, *A&A*, **486**, 545
9. R. Tylenda 2003, in: S. Kwok, M. Dopita, & R. Sutherland (eds.), *Hot Haloes of Planetary Nebulae*, Proc. IAU Symposium No. 209, 451